



Article

Effects of Temperature on the Relationship between Mode-I Fracture Toughness and Tensile Strength of Rock

Gan Feng ^{1,2,3} , Xiao-chuan Wang ^{1,4,*} , Yong Kang ^{1,4}, Shi-gang Luo ³ and Yao-qing Hu ⁵

¹ Hubei Key Laboratory of Waterjet Theory and New Technology, Wuhan University, Wuhan 430072, China; fenggan@whu.edu.cn (G.F.); kangyong@whu.edu.cn (Y.K.)

² Department of Energy and Mineral Engineering, Pennsylvania State University, University Park, PA 16802, USA

³ The Key Laboratory of Safety for Geotechnical and Structural Engineering of Hubei Province, School of Civil Engineering, Wuhan University, Wuhan 430072, China; luosg009@sina.com

⁴ School of Power and Mechanical Engineering, Wuhan University, Wuhan 430072, China

⁵ Institute of Mining Technology, Taiyuan University of Technology, Taiyuan 030024, China; huyaoqing@tyut.edu.cn

* Correspondence: xcw001@whu.edu.cn

Received: 28 February 2019; Accepted: 27 March 2019; Published: 29 March 2019



Abstract: Fracture toughness is used to characterize rock resistance to fracturing and it is important in theoretical research and engineering applications. Mode-I fracture toughness can be predicted on the basis of an empirical relationship between fracture toughness (K_{IC}) and tensile strength (σ_t). In underground engineering, rocks are often subjected to different temperatures. Therefore, this paper explores the effect of temperature on the relationship between mode-I fracture toughness and tensile strength. The results show that the change trends in the K_{IC} and σ_t values of rocks at temperatures from 20 °C to 600 °C are broadly consistent with each other. For rocks heat-treated to the same temperature, the K_{IC} of the rock increases with an increase in σ_t . This positive correlation between K_{IC} and σ_t is different in rocks heat-treated to different temperatures. Critical crack propagation radius (r_{IC}) is an important factor in the relationship between K_{IC} and σ_t and is related to the type of rock and the conditions under which it is tested. For the same rock, r_{IC} is quite different after it has been exposed to different temperatures. The positive correlation between K_{IC} and σ_t results from a similarity in the fracture morphology and properties of failure when rock is destroyed in fracture and tensile tests.

Keywords: rock; fracture toughness; tensile strength; temperature; crack propagation radius

1. Introduction

Rock failure is very common in energy development engineering. The failure behavior of rocks affects the efficiency of the engineering project and may even be directly related to its success or failure. In some engineering applications, crack-formation is desirable, for instance in deep geothermal energy development where crack-formation in the artificial storage layer will increase the heat exchange area [1]. In such contexts, rock failure is conducive to improving the efficiency of energy extraction. In other engineering contexts, ensuring the stability and integrity of rock is essential to the smooth completion of the project. An example of this is in the rock surrounding underground coal gasification [2] or coal mining roadways [3]. Rock failure occurs through the initiation, development, and penetration of one or more cracks until macroscopic cracks are formed [4,5]. Cracks play a key role in rock failure, so the problem of rock failure can be analyzed by way of fracture mechanics.

Rock fracture mechanics can be used to identify and predict the imminent failure of rock mass structures, thereby providing vital information for improving the stability and safety of these structures [6]. Fracture toughness is an important parameter in fracture mechanics, as it reflects the ability of rock to resist fracturing [7–9]. Fracture toughness has been receiving a large amount of attention in theoretical research and engineering applications such as rock cutting, drilling, hydraulic fracturing, blasting, tunnel excavation, underground reservoir construction, and in-situ modified mining reservoir infiltration. This property has therefore become an important research object.

However, testing fracture toughness in an underground engineering context is practically difficult. Rocks deep in the formation can only be sampled by drilling, which requires high-tech drilling techniques and incurs high costs. Direct fracture toughness testing requires a large number of samples. The cores obtained by drilling are not only extremely small; they also have poor integrity. The sample is easily damaged during processing, and it is difficult to cut artificial notches of uniform size with precision [10]. Therefore, a simple, reasonable, economical, and efficient method for determining the fracture toughness of rock would be extremely helpful.

One proposed solution was that it should be possible to study the fracture behavior of rock through the relationships between fracture parameters and index test results [11]. This allows the fracture toughness value to be estimated on the basis of conventional mechanical parameters, thereby reducing core consumption. The relationship between fracture toughness and density has been studied [12]. There is a remarkably good match between normalized P-wave compressional velocity and the decreasing trend in normalized fracture toughness (K_{IC}) [13]. In addition, a method has been developed for quickly estimating the mode-I fracture toughness using point load testing [10]. Mode-I fracture is characterized by tensile stress perpendicular to the crack surface and relatively separated upper and lower surfaces. The study found that the fracture toughness of rock can be related to uniaxial compressive strength, uniaxial tensile strength, and point load strength index as well as rock density.

The mode-I fracture toughness of several types of rock and soil has been found to be directly proportional to their tensile strength [14,15]. Haberfield and Johnston [16] similarly investigated the relationship between tensile strength and mode-I fracture toughness for a wide variety of rocks and soils such as Melbourne mudstone, Johnstone, oil shale, granite, marble, micrite, basalt, and syenite. Their results showed a reasonably strong correlation between these two parameters. Harison et al. [17] showed a strong empirical relationship between mode-I fracture toughness and the tensile strength of soil using a ring test. Both the results of Haberfield and Johnston [16] and Harison et al. [17] can be expressed as

$$\sigma_t = a_0 K_{IC} \quad (1)$$

where a_0 is a constant. According to the comparisons made by Harison et al. [17], $a_0 = 15.4$ for the types of soil considered, and $a_0 = 13.6$ for the types of soft rock considered.

Further research has generated a large amount of experimental data showing a strong correlation between mode-I fracture toughness and tensile strength [18–21]. These experimental data were gathered using a variety of test methods, and many types of rock were tested. Some test data [18] were obtained under dynamic loading conditions while others were obtained under static or quasi-static loading. The tensile strength of rock varies considerably when measured by different methods, and the heterogeneity of the rock tested will influence the tensile strength value. Similar issues may arise with fracture toughness tests [22]. Therefore, it is necessary to assess the effect of each factor present in the experimental setup—such as the temperature, test method, loading rate, etc.—on the relationship between mode-I fracture toughness and tensile strength.

In summary, previous studies have obtained empirical formulas that are useful for estimating mode-I fracture toughness. However, these empirical formulas differ from each other. Furthermore, the results for mode-I fracture toughness calculated by these empirical formulas differ somewhat from experimental data. This is because important factors that are capable of causing significant changes in rock mechanics parameters are not considered. One such parameter is exposure to high temperature.

Many underground projects are located several kilometers below the surface of the earth, and the surrounding rocks are often in a high-temperature environment. The relationship between the mode-I fracture toughness and tensile strength of rock changes due to temperature and this effect on the mechanical parameters of the rock cannot be ignored, especially where temperatures are high. It is therefore necessary to consider the mode-I fracture toughness and tensile strength of rock at different temperatures and thereby use the correlations between them to achieve more accurate predictions of the mode-I fracture toughness value. Moreover, there has been a lack of in-depth research into the reasons behind the influence of temperature on the relationship between mode-I fracture toughness and tensile strength. Therefore, this article builds on previous research by testing the mode-I fracture toughness and tensile strength of rocks after heat-treatment to different temperatures. Theoretical analysis and mesoscopic observation are then used to study the effect of temperature on the correlation between mode-I fracture toughness and tensile strength.

2. Specimen Preparation and Test

2.1. Specimen Preparation

The rock used in this experiment was sandstone from Sichuan, China, with a density of 2.6 g/cm^3 . The elemental composition of the sandstone was measured by X-ray fluorescence (XRF). The results show that the most abundant oxide in the sandstone is SiO_2 , with an average value of 71.011%. This is followed by Al_2O_3 , which makes up 12.180% on average, and there are also small amounts of CaO , Fe_2O_3 , MgO , K_2O , and P_2O_5 . X-ray diffraction (XRD) experiments were carried out on samples of the sandstone to identify and quantify the mineral species present. The diffraction pattern is shown in Figure 1. The results show that the sandstone mainly consists of quartz, siliceous minerals, and feldspar, with a small amount of siderite and calcite.

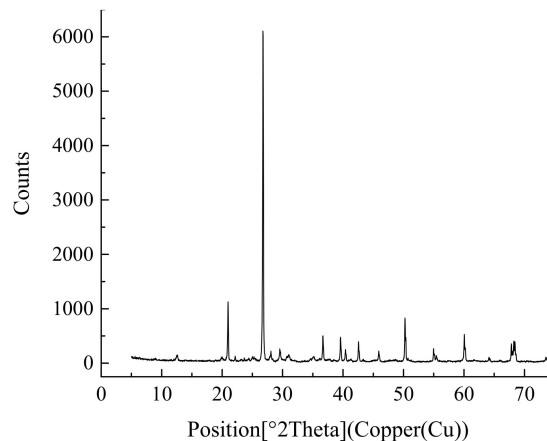


Figure 1. X-ray diffraction spectrum.

The tensile strength of the rock was determined by using the Brazilian splitting method, whereas fracture toughness was tested using the well-established method of three-point testing of a semi-circular bend (SCB) specimen with a central straight notch. The respective samples for these tests, as shown in Figure 2, were produced as follows. Rock cores—measuring 50-mm diameter and 50-mm thick—were drilled from the sandstone, as shown in Figure 2b. Some of the cylindrical cores were cut into discs with a diameter of 50 mm and a thickness of 25 mm as Brazilian disc specimens; these are shown in Figure 2c. Other cylindrical cores were machined into disc specimens with a diameter of 50 mm and a thickness of 20 mm and then cut into semi-circular disc samples. Since the thickness of the cutting blade causes a reduction in the size of the half-disc, only one half-disc that met the standard was derived from each whole disk. The SCB sample dimensions were determined according to the criteria recommended by the ISRM [6]. The dimensions of the SCB samples are shown in Table 1.

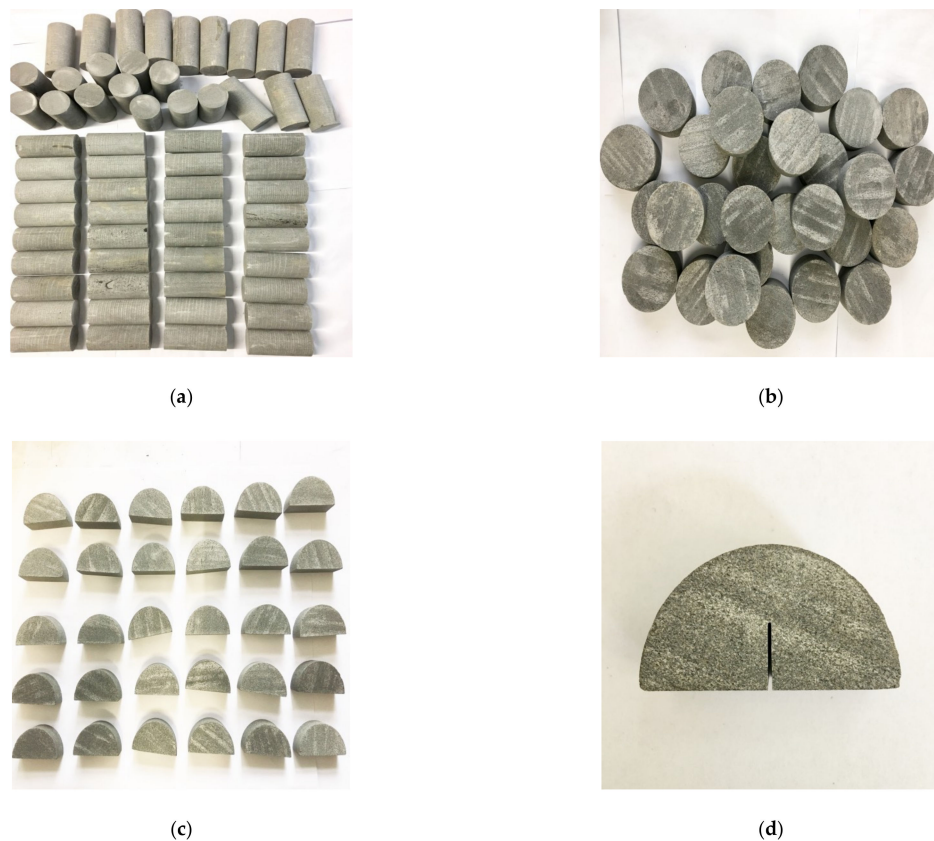


Figure 2. Processing and instruments. (a) Cylindrical samples; (b) Brazilian disc samples; (c) Micro milling; (d) Semi-circular bend sample.

Table 1. Geometrical dimensions of SCB specimens

Diameter (<i>D</i>)	Thickness (<i>B</i>)	Artificial-Notch Length (<i>a</i>)	Span Length (<i>S</i>)
50 mm	20 mm	12.5 mm	30.5 mm

The Brazilian disc samples and the semi-circular disc samples were placed in a muffle furnace for heating. The temperature gradient for the experiment was set to 100 °C, and a total of seven temperature points were set, room temperature (20 °C), 100 °C, 200 °C, 300 °C, 400 °C, 500 °C, and 600 °C. The heating rate was set to 5 °C /min. After the sample had been heated to the set temperature point, it was kept at that temperature for 10 hours to ensure sufficient heat-action time. Heating was then stopped, and the sample was allowed to cool naturally to room temperature in the muffle furnace. An artificial notch was cut in the semi-disc samples to make them into standard SCB samples. The artificial notch was 12.5 mm long and less than 2 mm wide. The samples and processing are shown in Figure 2.

2.2. Mode-I Fracture Toughness Test

The SCB samples were loaded into an Instron materials tester. In the displacement loading mode, the loading rate is 0.0002 mm/s, and the span of the two loading ends is 30.5 mm ($S = 30.5$ mm). The test results are automatically recorded by computer. The test loading system and assembly are shown in Figure 3.

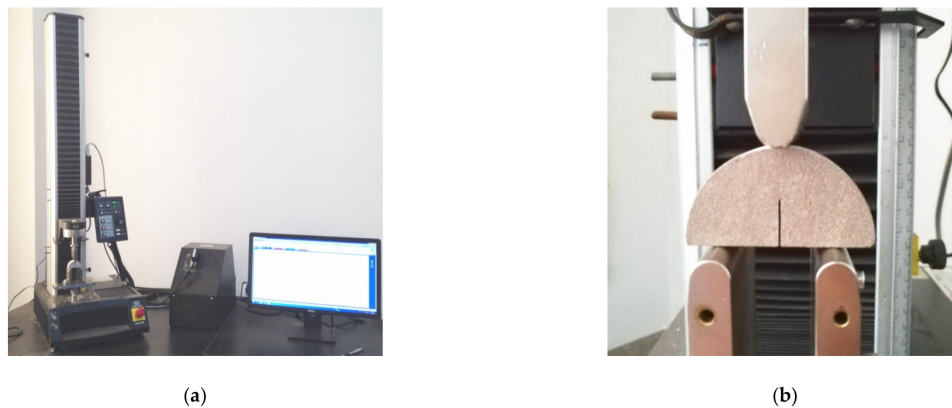


Figure 3. Experimental set-up for SCB tests. (a) Loading system; (b) Loading configuration.

The experimental results were calculated according to the method recommended by the ISRM [6], and the fracture toughness was calculated with the following formula.

$$K_{IC} = \frac{P_{\max} \sqrt{\pi a}}{2RB} Y' \quad (2)$$

$$Y' = -1.297 + 9.516(S/2R) - (0.47 + 16.457(S/2R))\beta + (1.071 + 34.401(S/2R))\beta^2 \quad (3)$$

$$\beta = a/R \quad (4)$$

where P_{\max} is the peak load at sample failure and Y' is the dimensionless stress intensity factor. The standards used in this paper are: $S/(2R) = 0.61$, $a/R = 0.5$.

2.3. Brazilian Disc Splitting Test

The rock mechanical property of tensile strength is of great significance for design, analysis, calculation, and evaluation in underground engineering. The tensile strength of rock is usually determined by the Brazilian disc splitting method. Brazilian disc splitting experiments were carried out at the School of Civil and Architectural Engineering at Wuhan University. The equipment used was the RMT-301 rock mechanic servo test machine, as shown in Figure 4a. A schematic for the test process is shown in Figure 4b.

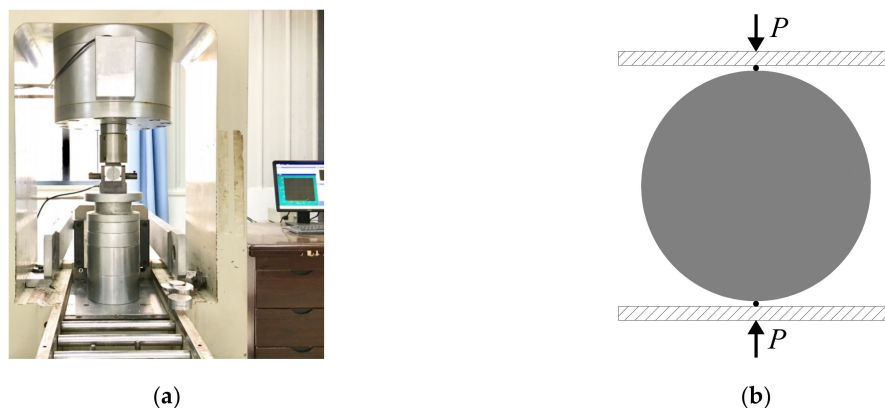


Figure 4. Brazilian disc splitting test. (a) BD splitting system; (b) Schematic of BD splitting.

The tensile strength of rock tested by the Brazilian disc splitting method is derived by way of the theory of elastic mechanics. The calculation formula [23,24] is

$$\sigma_t = \frac{2P_{\max}}{\pi DB} \quad (5)$$

where σ_t is the tensile strength of the rock, P_{max} is the load at the time of failure, D is the diameter of the Brazilian disc, and B is the thickness of the disc.

3. Test Results

3.1. Mode-I Fracture Toughness

Equation (2) was applied to calculate the mode-I fracture toughness from the data recorded in the SCB test. The average values of mode-I fracture toughness by processing temperature are plotted in Figure 5.

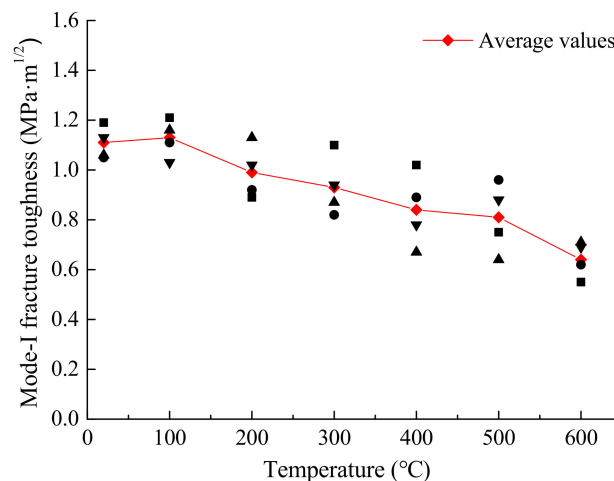


Figure 5. Mode-I fracture toughness of rock vs. temperature.

Figure 5 shows the average mode-I fracture toughness of the sandstone samples. In the range 20–500 °C, the mode-I fracture toughness was between 0.64 MPa·m^{1/2} and 1.13 MPa·m^{1/2}. These are relatively high values, and the range in variation is not large. Mode-I fracture toughness reached its highest value in the sample processed to 100 °C, slightly higher than that kept at 20 °C, indicating that heating to 100 °C had a toughening effect and made the rock more able to resist fracture. The lowest mode-I fracture toughness in the temperature range below 500 °C was at 500 °C, when it was 0.81 MPa·m^{1/2}; this is about 27.03% lower than at room temperature, indicating that heating to 500 °C had a weakening effect and made the rock less resistant to fracture.

When heat treatment was to higher than 500 °C, the mode-I fracture toughness suddenly decreased from 0.81 MPa·m^{1/2} for 500 °C to 0.64 MPa·m^{1/2} for 600 °C, a reduction by 20.99%. The mode-I fracture toughness of samples heated to 600 °C was 42.34% less than of those heated to 20 °C, indicating that exposure to such a high temperature had a very significant effect on fracture toughness, greatly weakening the ability of the rock to resist fracture. This can most probably be attributed to the fact that 573 °C, the transition temperature of α -quartz to β -quartz, lies within the temperature range 500–600 °C. This phase transition causes severe cracking in the rock structure, significantly impacting its mechanical properties.

3.2. Tensile Strength

Equation (5) was used to calculate the tensile strength of the rock from the data recorded in the Brazilian disc splitting tests. The average values are plotted in Figure 6.

Figure 6 shows the tensile strength of the sandstone after processing to the temperature steps from 20 °C to 600 °C, respectively. The tensile strength gradually decreased with an increase in processing temperature. The tensile strength decreased relatively slowly for samples processed at increasing temperatures from 20 °C to 500 °C, from 8.20 MPa for 20 °C to 6.62 MPa for 500 °C, a decrease of about 19.27%. When processed to a temperature in excess of 500 °C, the tensile strength of the samples

decreased sharply, decreasing by about 22.96% of the average 500 °C value at 600 °C. This shows that exposure to high temperature significantly reduced the tensile strength of the rock. In a study investigating the mode-I fracture toughness of three crystalline rocks, it has previously been shown that the two main mechanisms accounting for the reduced stiffness and toughness of rocks after heat-treatment are increasing micro-crack density and pulverization of minerals [25].

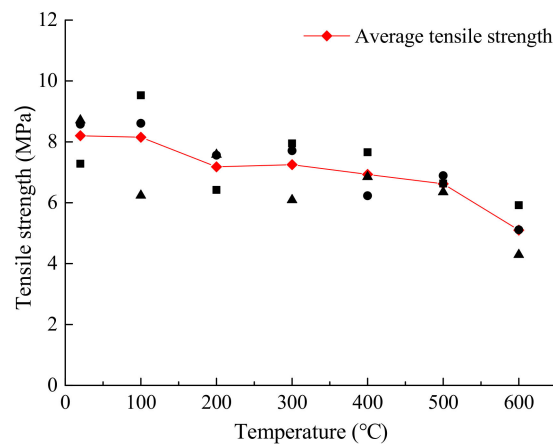


Figure 6. Tensile strength at different temperatures.

4. Relationship between K_{IC} and σ_t

4.1. Empirical Relationship

Underground engineering is carried out in a high-temperature environment, and temperature should therefore be a key consideration in such contexts. Exposure to high temperature will change the physical and mechanical properties of the rock [5,26–28]. Table 2 combines the results obtained in this study and experimental data obtained by other studies [18,29–31] regarding the effects of temperature on K_{IC} and σ_t . The K_{IC} test methods used in these other studies were SR for FS marble and FS gabbro, SCR3PB for Stripa granite, TPBSEN for BS granite, and SCB for Sichuan sandstone. Tensile strength was obtained via BD testing for FS marble, FS gabbro, Stripa granite, and Sichuan sandstone. In this paper, 25 °C is approximated as 20 °C.

Table 2. Fracture toughness and tensile strength of rock.

	FS Marble		FS Gabbro		Stripa Granite		BS Granite		SC Sandstone	
T	K_{IC}	σ_t	K_{IC}	σ_t	K_{IC}	σ_t	K_{IC}	σ_t	K_{IC}	σ_t
20	0.85	6.20	2.68	17.30	2.15	15.40	0.93	8.71	1.11	8.20
100	0.63	4.60	2.26	15.40	2.19	16.80	-	-	1.13	8.15
200	0.33	4.30	2.02	13.90	2.08	16.20	1.02	10.50	0.99	7.18
300	0.25	3.80	1.70	12.10	1.83	19.50	0.70	6.53	0.93	7.25
400	0.13	3.00	1.44	10.00	-	-	0.41	6.21	0.84	6.93
500	0.09	2.50	1.28	9.90	-	-	0.26	5.03	0.81	6.62
600	-	-	0.98	9.30	0.49	5.40	0.03	1.11	0.64	5.10

Table 2 shows that there is a large amount of variation in the mode-I fracture toughness and tensile strength of rocks treated to the same temperature in the different studies. This variation is due to differences in the rocks tested and test methods employed. In tests of the tensile strength of rock, the test method, rock heterogeneity, contact of the iron plate of the machine with the rock, etc., will all affect the test results. Results regarding the mode-I fracture toughness of rock will also be affected by such factors [22]. It can also be seen from Table 2 that both the mode-I fracture toughness

and the tensile strength gradually decrease with heating to greater temperature. This indicates that temperature exposure has an effect on mode-I fracture toughness and tensile strength. Straight-line relationships between the tensile strength and mode-I fracture toughness of rocks exposed to specific temperatures can be plotted on the basis of the data in Table 2 (Figure 7), and the expressions for these lines can be obtained by fitting.

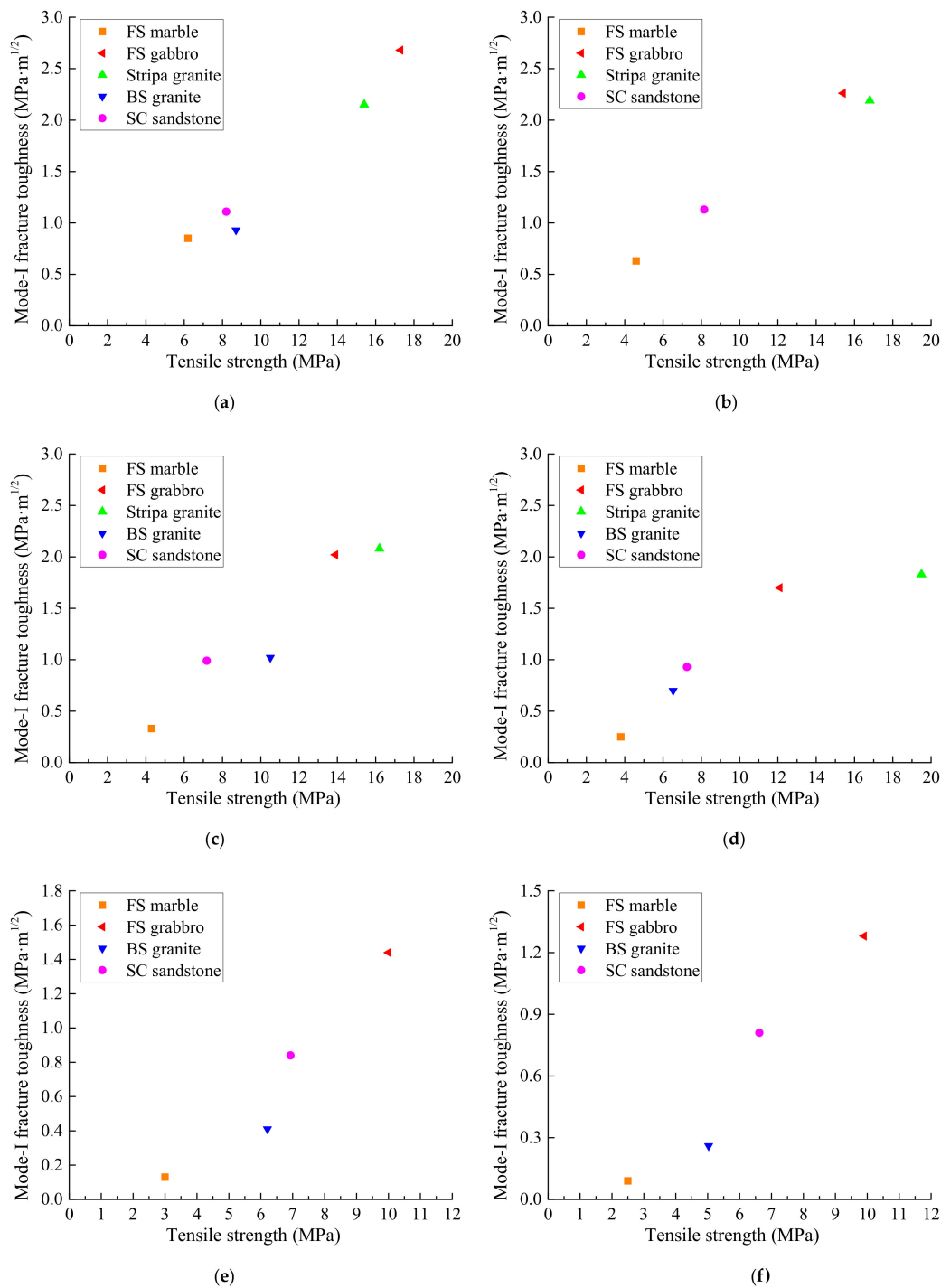


Figure 7. Cont.

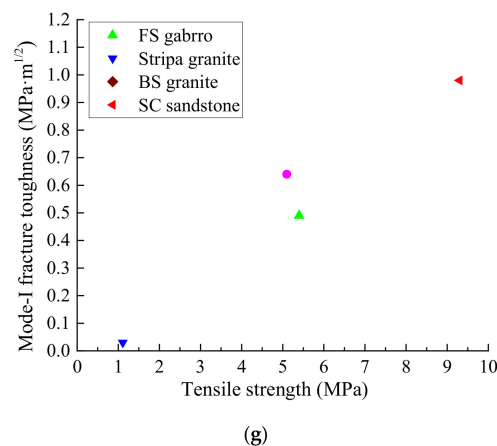


Figure 7. K_{IC} and σ_t of rock subjected to different temperatures. (a) 20 °C; (b) 100 °C; (c) 200 °C; (d) 300 °C; (e) 400 °C; (f) 500 °C; (g) 600 °C.

It can be seen from Figure 7 that, for rocks exposed to the same temperature, K_{IC} gradually increases with an increase in σ_t , making K_{IC} and σ_t broadly positively correlated. Table 3 gives the empirical formulas relating tensile strength and mode-I fracture toughness, where y represents mode-I fracture toughness and x represents tensile strength. The manner that K_{IC} varies with σ_t at each processing temperature is reflected by the slope of the fit line, termed the proportionality factor. In the linear fits, the proportionality factor for 20 °C, 0.1420, is the largest. That is, K_{IC} changes most with σ_t in rock exposed to this temperature. The proportionality factor for 600 °C is the smallest, 0.1054; that is, K_{IC} changes least with σ_t . Therefore, the positive correlation between K_{IC} and σ_t is different for rock that has been exposed to different temperatures. There are also differences in the fitting coefficient R^2 . For processing to 20 °C, 100 °C, 200 °C, and 600 °C, the fitting coefficients R^2 were 0.94, 0.98, 0.90, and 0.95, respectively, for all of which $R^2 \geq 0.90$. K_{IC} and σ_t thus show a very obvious linear relationship under these processing conditions. For processing temperatures ranging from 300 °C to 500 °C, the fitting coefficient ranged from 0.77 to 0.85. These coefficients reflect a less pronounced linear relationship between K_{IC} and σ_t . Thus, when rocks are heated to room temperature, 100 °C, 200 °C, and 600 °C, the linear relationship is more pronounced than when they are heated to between 300 °C and 500 °C, and temperature exposure has a significant effect on the relationship between the mode-I fracture toughness and tensile strength of rock. To achieve better fits, we also considered exponential formulas relating mode-I fracture toughness and tensile strength. The expression of the exponential function is different at different temperatures. $R^2 > 0.90$ at 20 °C, 100 °C, 400 °C, and 500 °C. Therefore, at these temperatures, the mode-I fracture toughness has a good exponential relationship with the tensile strength. Comparing the linear function with the exponential function, the exponential function achieves a better description of the relationship between the mode-I fracture toughness and the tensile strength at 20 °C, 400 °C, and 500 °C, whereas the linear function achieves a better description at 100 °C, 200 °C, 300 °C, and 600 °C. Specifically, for example, at 400 °C, the R^2 of the exponential function is significantly larger than that of the linear function, and therefore, it is more accurate to predict the K_{IC} value using an exponential function. From the above analysis, it can be concluded that although the mode-I fracture toughness is positively correlated with the tensile strength, their relational expressions differ at different temperatures.

Through analysis of the abundant testing data available regarding both rock fracture toughness and rock tensile strength values, an empirical relationship has been established between the two parameters [18] that can be expressed by the following equation

$$\sigma_t = 6.88K_{IC} \quad (6)$$

with a coefficient of determination $R^2 = 0.94$.

A linear empirical relationship has also been identified between the K_{IC} and σ_t of a particular clay [19]

$$K_{IC} = 0.3546\sigma_t \quad (7)$$

More broadly, the correlation between K_{IC} and σ_t can be expressed as

$$K_{IC} = \alpha\sigma_t \quad (8)$$

where α =the proportionality coefficient. The proportionality coefficient is different for different soils or rocks and testing methods.

Further analysis has indicated that the relationship between tensile strength and fracture toughness is actually of power-law type [20]

$$K_{IC} = \alpha\sigma_t^n \quad (9)$$

instead of the linear type shown in Equation (8) and that this relationship only becomes linear for the particular case where exponent n is equal to 1.

Table 3. Fitting formulas for different temperatures

T (°C)	Linear Formula	R^2	Exponential Formula	R^2
20	$y = 0.1420x$	0.9448	$y = 0.4288\exp(0.1049x)$	0.9728
100	$y = 0.1379x$	0.9821	$y = 0.4328\exp(0.1025x)$	0.9637
200	$y = 0.1274x$	0.9035	$y = 0.2376\exp(0.1444x)$	0.8713
300	$y = 0.1077x$	0.8457	$y = 0.2959\exp(0.1100x)$	0.7027
400	$y = 0.1184x$	0.7721	$y = 0.0508\exp(0.3512x)$	0.9421
500	$y = 0.1129x$	0.8163	$y = 0.0430\exp(0.3687x)$	0.9184
600	$y = 0.1054x$	0.9478	$y = 0.0335\exp(0.4255x)$	0.8092

4.2. Theoretical Analysis

Theoretical analysis was conducted to explore the correlation between the mode-I fracture toughness and tensile strength of rock further. The stress field near the crack tip when a rock is subjected to biaxial tensile stress can be considered in terms of fracture mechanics [32] as shown in Figure 8.

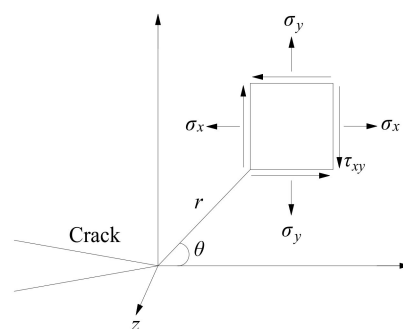


Figure 8. Stress near the crack tip.

According to elastic mechanics [33], the stress field near the crack tip can be approximated as

$$\sigma_x = \frac{K_I}{\sqrt{2\pi r}} \cos \frac{\theta}{2} \left(1 - \sin \frac{\theta}{2} \sin \frac{3\theta}{2} \right) \quad (10)$$

$$\sigma_y = \frac{K_I}{\sqrt{2\pi r}} \cos \frac{\theta}{2} \left(1 + \sin \frac{\theta}{2} \sin \frac{3\theta}{2} \right) \quad (11)$$

$$\tau_{xy} = \frac{K_I}{\sqrt{2\pi r}} \cos \frac{\theta}{2} \sin \frac{\theta}{2} \cos \frac{3\theta}{2} \quad (12)$$

If the area around the crack tip does not undergo significant plastic deformation, it is considered to be an inelastic stress region when micro-cracks occur. The principal stress of the area near the crack tip can be expressed by elastic mechanics as

$$\sigma_1 = \frac{\sigma_x + \sigma_y}{2} + \sqrt{\left(\frac{\sigma_x - \sigma_y}{2}\right)^2 + \tau_{xy}^2} \quad (13)$$

$$\sigma_2 = \frac{\sigma_x + \sigma_y}{2} - \sqrt{\left(\frac{\sigma_x - \sigma_y}{2}\right)^2 + \tau_{xy}^2} \quad (14)$$

where σ_1 is the maximum principal stress. Substituting Equations (10–12) into Equation (13)

$$\sigma_1 = \frac{K_I}{\sqrt{2\pi r}} \cos \frac{\theta}{2} \left(1 + \sqrt{2} \sin \frac{\theta}{2} \cos \frac{3\theta}{2}\right) \quad (15)$$

Previous research has identified the following main material fracture criteria: the maximum circumferential tensile stress criterion, strain energy density criterion, maximum energy release rate criterion, and modified maximum tangential stress (MMTS) criterion [11,34–37]. However, the experimental results available show that, for rocks, fracture toughness is controlled by the maximum principal stress (i.e., tensile strength) [11] and the expansion of microcracks is one of the causes of rock damage [11,26,38–42]. Microcrack propagation is caused by the microcrack being subjected to tensile stress rather than compressive stress or shear stress. Moreover, rock exhibits brittle properties, and the tensile strength is much smaller than the compressive strength. When the tensile stress in the rock exceeds the maximum tensile stress, damage will occur. Therefore, the condition of the maximum tensile stress being equal to the tensile strength, $\sigma_1 = \sigma_t$, can be considered a critical case [21]. When the stress intensity factor at the crack tip reaches a critical value, the crack expands, that is, $K_I = K_{IC}$. If crack tip strength failure and crack initiation are used as equivalent criteria, the crack propagation radius reaches the critical crack propagation radius, that is, $r = r_{IC}$. Equation (15) can be then be rewritten as

$$\sigma_t = \frac{K_{IC}}{\sqrt{2\pi r_{IC}}} \cos \frac{\theta}{2} \left(1 + \sqrt{2} \sin \frac{\theta}{2} \cos \frac{3\theta}{2}\right) \quad (16)$$

The crack propagation angle (θ) is the direction of crack propagation. For a pure mode-I crack, the crack propagation angle $\theta = 0^\circ$. Therefore, Equation (16) can be written as [21]

$$\frac{K_{IC}}{\sigma_t} = \sqrt{2\pi r_{IC}} \quad (17)$$

However, Equation (17) only shows a positive correlation between mode-I fracture toughness (K_{IC}) and tensile strength (σ_t), and cannot be used to accurately estimate the critical crack propagation radius (r_{IC}). Instead, it is necessary to determine it empirically, as Equation (17) indicates that it should be possible to determine the ratio of K_{IC} to σ_t for the same rock subject to the same conditions and using the same test method and sample type. That is, the critical crack extension radius (r_{IC}) should be a constant. Specifically, the value of r_{IC} is related to the type of rock and the conditions (e.g., temperature, humidity). The effect of temperature on the crack propagation radius is shown in Table 4.

Table 4 shows that the r_{IC} value varies from 0.00021 m to 0.00299 m for FS marble, 0.00177 m to 0.00382 m for FS gabbro, 0.00131 m to 0.00310 m for SP granite, 0.00012 m to 0.00183 m for BS granite, and 0.00234 m to 0.00306 m for SC sandstone. Thus, the r_{IC} values of different rock types are different. In the temperature dimension, the maximum values of the r_{IC} of FS marble, FS gabbro, SP granite, BS granite, and SC sandstone were 1323.81%, 115.82%, 136.64%, 1425.00%, and 30.77% above the minimum values, respectively. That is, for the same rock, the r_{IC} values differ greatly for

samples exposed to different temperatures: temperature exposure has a significant effect on the crack propagation radius r_{IC} at the time of rock fracture. However, the test values for K_{IC} and σ_t can be influenced by numerous factors (e.g., the loading rate, test method, and sample type), so it may not be possible to acquire an exact value for the critical crack propagation radius r_{IC} through evaluation of K_{IC} and σ_t .

The K_{IC} of the rock has a linear proportional relationship with σ_t , and the proportionality coefficient is related to the crack propagation radius (r_{IC}). Experimental data can be used to statistically determine the average r_{IC} value of various rocks exposed to different temperatures.

Table 4. The r_{IC} value (m) for different processing temperatures.

T (°C)	FS Marble	FS Gabbro	SP Granite	BS Granite	SC Sandstone
25	0.00299	0.00382	0.00310	0.00181	0.00292
100	0.00299	0.00343	0.00270	-	0.00306
200	0.00094	0.00336	0.00262	0.00150	0.00303
300	0.00069	0.00314	0.00140	0.00183	0.00262
400	0.00030	0.00330	-	0.00069	0.00234
500	0.00021	0.00266	-	0.00043	0.00238
600	-	0.00177	0.00131	0.00012	0.00251

5. Discussion

5.1. Fracture Analysis

The fracture morphology in rock failure is related to the rock type and the conditions the rock is under (e.g., temperature, humidity, loading rate, and confining pressure). The fracture morphology records the irreversible shape of the rock fracture and provides information about crack initiation, propagation, penetration, and failure. Therefore, the properties of rock failure can be inferred by examining and analyzing the fracture morphology. The results of this analysis can then be fed back to engineering as a valuable reference for practical production. Scanning electron microscopy (SEM) can reveal the shape of the fracture clearly and is commonly applied for research into rock fractures [4,27]. After rock failure had occurred in the present study, the fracture was examined by SEM; the photographs obtained are shown in Figure 9.

The SEM image of the sample exposed only to room temperature (20 °C) shows a relatively flat fracture surface with almost no discrete cracks (Figure 9a). As samples are exposed to increasingly high temperatures, the Brazilian splitting and SCB fracture surfaces gradually become rougher, as shown in Figure 9b–f. A river-like pattern can be observed clearly in both BD and SCB samples, as shown in Figure 9b,c. The river-like pattern originates from the grain boundaries, and as cracks develop, it spreads throughout the mineral particles. As the exposure temperature increases, the range of the pattern is larger and the surface is rougher. A tear-like fracture pattern is caused by temperature and load, and the crack changes direction and tears in a relatively weak layer. The tear-like fracture pattern was observed in both the BD and SCB samples, as shown in Figure 9e,f. River-like and tear-like fractures are mainly formed by tensile failure. Where the main crack surface is perpendicular, breakage occurs due to uncoordinated deformation of weak mineral particles or cement. The fractured areas become interconnected and penetrate to form a fractured structure, as shown in Figure 9d. The action of high temperature causes significant uncoordinated deformation between the mineral particles in the rock and between the particles and the cement. Large quantities of cracks are generated, and the structure seriously deteriorates. The failure of rocks is a process in which the various sub-parts of the rock break through and form large macroscopic cracks.

It can be seen from the above analysis that the fracture morphology in the K_{IC} and σ_t tests is very similar, and the failure mechanism is the same. Temperature has a significant effect on the morphology of the rock fracture. This is because, as the temperature increases, the thermal motion of mineral particles, crystals, and atoms in the sandstone gradually increases. The number of weak crystal faces of

the minerals inside the rock increases, and the potential for local plastic deformation increases. These factors result in the formation of river-like and tear-like fracture patterns. Moreover, as the temperature increases, the internal structure of the rock gradually deteriorates, and the numbers of pores and cracks gradually increase. This is an important reason for the decline in the mechanical properties of the rock.

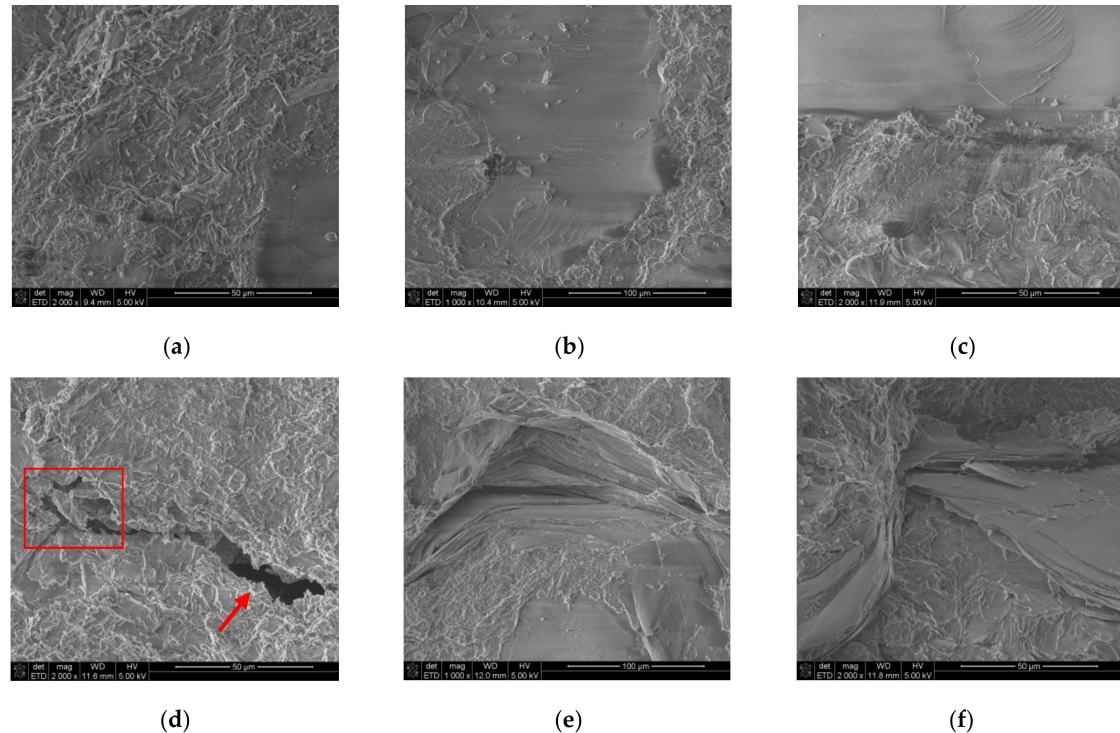


Figure 9. SEM fractography of fractures in sandstone (the red box indicates fragmentation, and the arrow indicates a pore). (a) BD fracture (20 °C); (b) BD fracture (300 °C); (c) SCB fracture (300 °C); (d) SCB fracture (600 °C); (e) SCB fracture (600 °C); (f) BD fracture (600 °C).

5.2. Influence of Temperature on K_{IC} and σ_t

It can be seen from Figures 5 and 6 that temperature has a significant influence on the mode-I fracture toughness and tensile strength of the rock. In the temperature range 20–100 °C, the mode-I fracture toughness of sandstone increases slightly, showing a toughening effect, and the tensile strength is almost unchanged. In general, the mechanical properties of Sichuan sandstones are not significantly changed by heating to temperatures below 100 °C. Figures 10 and 11 respectively show the variation in the mode-I fracture toughness and in the tensile strength of different types of rocks with temperature.

It is apparent from Figures 10 and 11 that there is significant scatter in the change trends in fracture toughness and tensile strength with temperature. As rock is exposed to higher temperatures, the tensile strength decreases first because microcracks are generated and then via plastic deformation [43]. A decrease in the fracture toughness of gabbro with heat-treatment to temperatures from 20 °C to 100 °C is probably due to structural and mineralogical changes in the rock [44]. Heat-treating rocks to 100 °C resulted in reduced fracture toughness due to the development of tensile stress caused by the uncoordinated expansion of mineral particles in the rock and the consequent development of microcracks. Under the action of heat, the rock mineral particles gradually expand and the volume increases. For non-compact rocks, an increase in mineral particle volume reduces the volume of original voids and enhances extrusion between mineral particles, which in turn enhances the mechanical properties of the rock. Heating also causes free water in the rock to evaporate, and frictional resistance increases as the particles become dry, which also leads to an increase in mechanical properties. Of course, the generation of thermal cracks will also weaken the mechanical properties of the rock. Observing the SEM picture of Sichuan sandstone, rock samples at room temperature and 100 °C are

relatively intact, and pores and fissures are rarely seen. It can be seen that at 100 °C, the effect of thermal cracking is not dominant, and volume expansion is likely to be more dominant. Therefore, the mechanical properties of the rock will be slightly enhanced.

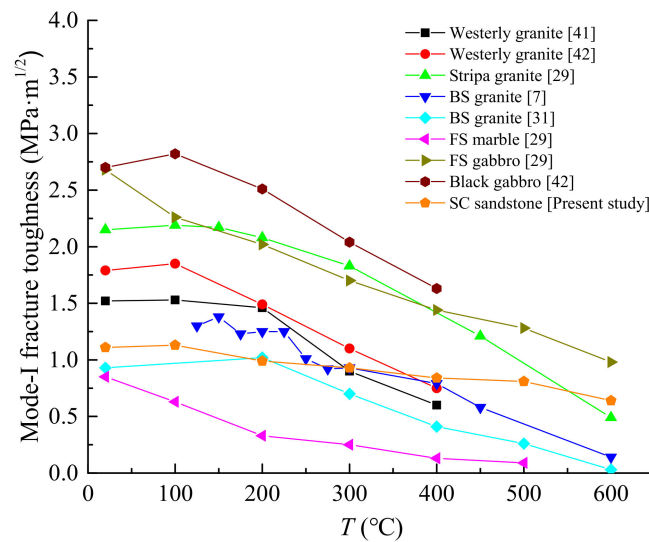


Figure 10. Variation in rock mode-I fracture toughness with temperature.

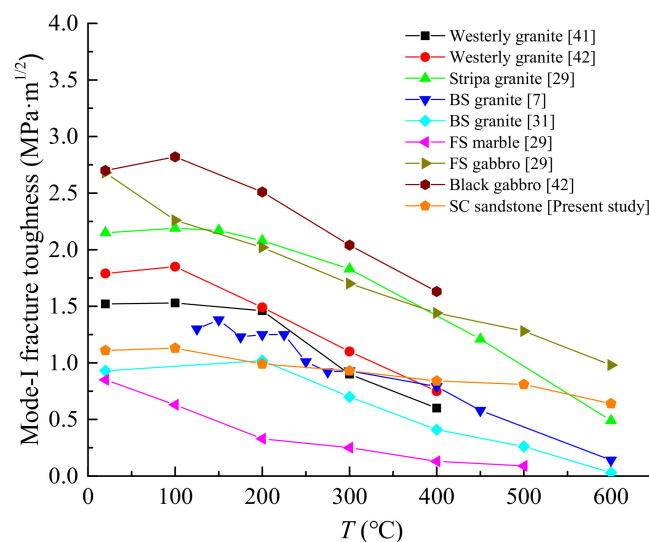


Figure 11. Variation in rock tensile strength with temperature.

At temperatures above 100 °C, the mode-I fracture toughness and tensile strength of the rock are reduced, mainly due to thermal cracking of the rock structure. As the temperature rises, the thermal expansion coefficient of the mineral particles changes; the thermal deformation is not coordinated, and cracks are generated. Thermal stress caused by an uneven temperature distribution also causes tensile cracks to form. After rock has been subjected to heat, the cracks formed inside it are still present after cooling and are irreversible [27]. It can be observed from the SEM image that exposure to temperatures above 100 °C increased the number of cracks and pores in the rock, which leads to the gradual weakening of its properties. The structural damage caused to the rock by the heat is a result of both physical and chemical reactions such as dehydration release of bound water from crystals, conversion between homogeneous polymorphs of quartz, mineral decomposition reactions, and thermal expansion. In particular, large pores are formed at high temperatures above 500 °C, when the conversion of α -quartz to β -quartz causes severe cracking of the structure, as shown in Figure 9.

High temperatures cause structural fragmentation of the rock. This is the direct cause of the reduced mode-I fracture toughness and tensile strength of the rock.

5.3. Reasons for the Relationship between K_{IC} and σ_t

The mechanical parameters of rock may not be isolated, as they are, to an extent, related to each other. In underground energy development, rock masses are often in complex stress states. For example, tunnels, engineering slopes, underground engineering chambers, and roadways are in a state of tensile stress, while other parts of the system are in a state of compressive stress. Since the tensile strength of the rock is much lower than the compressive strength, the rock always begins to be damaged in zones under tensile stress. Cracks change their propagation direction, and fracture surfaces separate because the tensile stress exceeds the bonding force between the atoms, leading to rock failure, that is, mode-I fracture. Some research [45,46] has been carried out into the properties of tensile crack extension under compressive shear stress conditions. It is believed that cracks always undergo mode-I fracturing by turning. When rock in compression is damaged, shearing and stretching are mainly caused by tensile cracks induced by tensile stress. This is one of the reasons why tensile, shear, and compressive strength are interrelated.

Tensile damage may also occur when rock is in a compressed state. Rocks are brittle materials, and tensile stress can easily cause damage. Some scholars have studied microscopic fracturing in a compressed state. The results show that stress-induced microcracks in the rock are caused by tensile failure, not by shear failure. Crack propagation in the axial direction is caused by tensile failure and has hysteresis [47–49]. The above results indicate that the tensile strength and compressive strength of rock are correlated and that compressive and tensile failure has similar fracture mechanisms at microscopic scales, so one of the root causes of rock failure is the generation and expansion of microcracks. The generation and expansion of microcracks occurs due to tensile stress and, ultimately, tensile failure [38–40]. However, it has been argued that the tensile strength of axial cracks is the primary control over compression damage [47] and that the characteristics of macro-cracks in brittle rock-like materials are not solely determined by the nature of micro-cracks. In the SCB test, the stress resulting from compression is concentrated at the loading point and the tip of the artificial notch. Tensile stress causes a new crack or an existing axial crack to spread gradually from the notch tip. Eventually, the SCB sample is broken into two halves along the main tensile crack, as shown in Figure 12a. In the Brazilian splitting test, the loading point of the Brazilian disc is compressed, causing tensile stress on both sides of the center of the disc. The tensile action caused by the tensile stress between the two points causes tensile cracking at the fracture surface. The expansion and penetration of the main tensile crack eventually lead to the destruction of the rock, breaking it into two halves as shown in Figure 12b. After being heat-treated at temperatures between 20 °C and 600 °C, it was observed that all of the SCB and BD samples were broken into two halves. This means that differences in the temperature of heat-treatment did not affect this characteristic of failure along a main central tensile crack.



Figure 12. Broken specimens. (a) Broken sample of SCB; (b) Broken sample of BD

The fracture morphology is related to the loading process and is ultimately determined by the properties of fracturing. The similarity of the SEM-detected fracture morphology under the two testing methods is due to their failure properties being the same. The characteristics of cracks in SCB specimens and Brazilian splitting specimens are similar [18]. This similarity indicates that the mechanical process by which the damage occurs is the same. The tensile toughness of the rock can be estimated by testing the tensile strength of the sample, which will greatly simplify fracture toughness evaluation. Indeed, a linear correlation is to be expected between the fracture toughness and tensile strength of a rock on the basis of the observation that the fracture surfaces of rocks in a fracture test are similar to those following tensile failure in a tension test [18]. SEM observations were made of the fracture surfaces of the SCB and BD samples after heat-treatment at different temperatures (20–600 °C). At the same temperature, microscopic analysis shows that the fracture morphology of specimens subjected to the two tests is similar, displaying the same failure properties and indicating that fracturing occurs by the same mechanism in the two tests.

The two parameters, mode-I fracture toughness and tensile strength, both reflect the ability of the rock to resist breaking, and this study has shown that the variation of mode-I fracture toughness and tensile strength with exposure to higher temperatures is basically the same.

6. Conclusions

In this paper, experimental and theoretical analyses of the mode-I fracture toughness and tensile strength of sandstone exposed to different temperatures were carried out. The main conclusions drawn are as follows:

(1) The mode-I fracture toughness and tensile strength of rock decrease slowly with temperature from 20 °C to 500 °C. They reduce much more drastically between 500 °C and 600 °C. The change trends of mode-I fracture toughness and tensile strength with temperature are basically consistent with each other. This is because high temperatures damage the interior of the rock and gradually create pores and cracks. When rock is subjected to temperatures above 500 °C, the cracking of the rock is more serious, and a fragmentation structure forms. These effects cause the two parameters to change significantly as the temperature increases.

(2) Both theoretically and experimentally, the mode-I fracture toughness of rock is positively correlated with tensile strength; that is, the fracture toughness increases with the increase of tensile strength. At some temperatures, the relationship between mode-I fracture toughness and tensile strength is well suited for description with a proportional function. At other temperatures, an exponential function provides a more accurate description. The relational expressions differ at different temperatures. Therefore, temperature has a significant effect on the relationship between mode-I fracture toughness and tensile strength.

(3) The relationship between mode-I fracture toughness and tensile strength is affected by the crack propagation radius (r_{IC}). r_{IC} is related to the type of rock and is affected by temperature. For the same rock, the r_{IC} is different after heat treatment at different temperatures.

(4) Both the SCB and BD samples failed along a main central tensile crack. The features of the failure were the same; that is, they split into two halves. SEM observation of the fractures further shows that, at the same temperature, the fracture morphology of SCB and Brazilian splitting samples after failure is similar. For example, river-like patterns were observed on both BD and SCB samples that had been heated to 300 °C, and a layered tear-like pattern was observed in samples heated to 600 °C. This mesoscopic morphological similarity between samples subjected to the two tests confirms they have the same failure properties.

Author Contributions: G.F. performed the experiments, data analyses, and manuscript writing; X.W. designed the experiments and helped to analyze the results; Y.K., S.L. and Y.H. analyzed the results and revised this manuscript.

Acknowledgments: This study was supported by the National Key Basic Research and Development Program of China (973 Program) (grant no. 2018YFC0808401) and the National Natural Science Foundation of China (grant no. 51574173).

Conflicts of Interest: The authors declare no conflict of interest.

Abbreviations

SCB	Semi-circular bend
BD	Brazilian disc
SEM	Scanning electron microscopy
ISRM	International Society for Rock Mechanics
R	SCB sample radius (mm)
B	SCB and Brazilian disc sample thickness (mm)
a	Artificial-notch length (mm)
S	Support span (mm)
P	Load (N)
D	SCB sample diameter (mm)
K_{IC}	Mode-I fracture toughness ($\text{MPa}\cdot\text{m}^{1/2}$)
P_{\max}	Peak load of specimen failure (N)
γ'	Dimensionless stress intensity factor
UCS	Uniaxial compressive strength (MPa)
BTS	Brazilian tensile strength (MPa)
T	Temperature ($^{\circ}\text{C}$)
σ_t	Tensile strength (MPa)
XRF	X-ray fluorescence
XRD	X-ray diffraction
FS	Fangshan (in the suburb of Beijing)
BS	Beishan (in Gansu province, China)
SC	Sichuan (in Sichuan province, China)
TPBSEN	Three-point bending single edge-notched
SCR3PB	Single crack rod three-point bending
R^2	Coefficient of determination
θ	Crack propagation angle ($^{\circ}$)
r	Crack propagation radius (m)
r_{IC}	Critical crack propagation radius (m)
σ_x	Normal stress in the x -direction (MPa)
σ_y	Normal stress in the y -direction (MPa)
τ_{xy}	Shear stress (MPa)
σ_1	Maximum principal stress (MPa)
σ_2	Minimum principal stress (MPa)

References

1. Cui, G.D.; Ren, S.R.; Zhang, L.; Ezekiel, J.; Enechukwu, C.; Wang, Y.; Zhang, R. Geothermal exploitation from hot dry rocks via recycling heat transmission fluid in a horizontal well. *Energy* **2017**, *128*, 366–377. [\[CrossRef\]](#)
2. Su, F.; Hamanaka, A.; Itakura, K.; Deguchi, G.; Sato, K.; Kodam, J. Evaluation of coal Combustion zone and gas energy recovery for underground coal gasification (UCG) process. *Energy Fuels* **2017**, *31*, 154–169. [\[CrossRef\]](#)
3. Zhang, Z.T.; Zhang, R.; Xie, H.P.; Gao, M.Z.; Xie, J. Mining-induced coal permeability change under different mining layouts. *Rock Mech. Rock Eng.* **2016**, *49*, 3753–3768. [\[CrossRef\]](#)
4. Feng, G.; Kang, Y.; Meng, T.; Hu, Y.Q.; Li, X.H. The influence of temperature on mode I fracture toughness and fracture characteristics of sandstone. *Rock Mech. Rock Eng.* **2017**, *50*, 2007–2019. [\[CrossRef\]](#)
5. Feng, G.; Kang, Y.; Chen, F.; Liu, Y.W.; Wang, X.C. The influence of temperature on mixed-mode (I+II) and mode-II fracture toughness of sandstone. *Eng. Fract. Mech.* **2018**, *189*, 51–63. [\[CrossRef\]](#)
6. Kuruppu, M.D.; Obara, Y.; Ayatollahi, M.R.; Chong, K.P.; Funatsu, T. ISRM-suggested method for determining the mode I static fracture toughness using semi-circular bend specimen. *Rock Mech. Rock Eng.* **2013**, *47*, 267–274. [\[CrossRef\]](#)

7. Zuo, J.-P.; Wang, J.-T.; Sun, Y.-J.; Chen, Y.; Jiang, G.-H.; Li, Y.-H. Effects of thermal treatment on fracture characteristics of granite from Beishan, a possible high-level radioactive waste disposal site in China. *Eng. Fract. Mech.* **2017**, *182*, 425–437. [\[CrossRef\]](#)
8. Ayatollahi, M.R.; Zakeri, M. An improved definition for mode I and mode II crack problems. *Eng. Fract. Mech.* **2017**, *175*, 235–246. [\[CrossRef\]](#)
9. Monfared, M.M.; Ayatollahi, M. Interactions of multiple cracks in a transversely isotropic piezoelectric plane under mixed mode condition. *Eng. Fract. Mech.* **2017**, *180*, 87–104. [\[CrossRef\]](#)
10. Bearman, R.A. The use of the point load test for the rapid estimation of mode I fracture toughness. *Int. J. Rock Mech. Min. Sci.* **1999**, *36*, 257–263. [\[CrossRef\]](#)
11. Whittaker, B.N.; Singh, R.N.; Sun, G. *Rock Fracture Mechanics—Principles, Design and Applications*; Elsevier Science Publisher: Amsterdam, the Netherlands, 1992.
12. Brown, G.; Reddish, D. Experimental relations between rock fracture toughness and density. *Int. J. Rock Mech. Min.* **1997**, *34*, 153–155. [\[CrossRef\]](#)
13. Nasser, M.H.B.; Schubnel, A.; Young, R.P. Coupled evolutions of fracture toughness and elastic wave velocities at high crack density in thermally treated Westerly granite. *Int. J. Rock Mech. Min. Sci.* **2007**, *44*, 601–616. [\[CrossRef\]](#)
14. Gunsallus, K.L.; Kulhawy, F.H. A comparative evaluation of rock strength measures. *Int. J. Rock Mech. Min. Sci. Geomech. Abstr.* **1984**, *21*, 233–248. [\[CrossRef\]](#)
15. Bhagat, R.B. Mode I fracture toughness of coal. *Int. J. Min. Eng.* **1985**, *3*, 229–236. [\[CrossRef\]](#)
16. Haberfield, C.; Johnston, I. Relationship between fracture toughness and tensile strength for geomaterials. In Proceedings of the 12th International Conference on Soil Mechanics and Foundation Engineering (SMFE 1989), Rio De Janeiro, Brazil, 13–18 August 1989; pp. 47–52.
17. Harison, J.A.; Hardin, B.O.; Mahboub, K. Fracture toughness of compacted cohesive soils using ring test. *J. Geotech. Eng.* **1994**, *120*, 872–891.
18. Zhang, Z.X. An empirical relation between mode I fracture toughness and the tensile strength of rock. *Int. J. Rock Mech. Min. Sci.* **2002**, *39*, 401–406. [\[CrossRef\]](#)
19. Wang, J.-J.; Zhu, J.-G.; Chiu, C.; Zhang, H. Experimental study on fracture toughness and tensile strength of clay. *Eng. Geol.* **2007**, *94*, 65–75. [\[CrossRef\]](#)
20. Lakshmikantha, M.R.; Prat, P.C.; Ledesma, A. Discussion on “Experimental study on fracture toughness and tensile strength of a clay” [Engineering Geology 94 (2007) 64–75]. *Eng. Geol.* **2008**, *101*, 295–296. [\[CrossRef\]](#)
21. Deng, H.F.; Zhu, M.; Li, J.L.; Wang, Y.; Luo, Q.; Yuan, X.F. Study of mode-I fracture toughness and its correlation with strength parameters of sandstone. *Rock Soil Mech.* **2012**, *33*, 3585–3591. (In Chinese)
22. Hudson, J.A.; Brown, E.T.; Rummel, F. The controlled failure of rock discs and rings loaded in diametral compression. *Int. J. Rock Mech. Min. Sci. Geomech. Abstr.* **1972**, *9*, 241–248. [\[CrossRef\]](#)
23. Bieniawski, Z.T.; Hawkes, I. Suggested methods for determining tensile strength of rock materials. *Int. J. Rock Mech. Min. Sci. Geomech. Abstr.* **1978**, *15*, 99–103.
24. Gholami, R.; Rasouli, V. Mechanical and elastic properties of transversely isotropic slate. *Rock Mech. Rock Eng.* **2014**, *47*, 1763–1773. [\[CrossRef\]](#)
25. Talukdar, M.; Guha, D.; Singh, T.N. Correlating mode-I fracture toughness and mechanical properties of heat-treated crystalline rocks. *J. Rock Mech. Geotech. Eng.* **2018**, *10*, 91–101. [\[CrossRef\]](#)
26. Yin, T.; Li, X.; Cao, W.; Xia, K. Effects of thermal treatment on tensile strength of Laurentian granite using Brazilian test. *Rock Mech. Rock Eng.* **2015**, *48*, 2213–2223. [\[CrossRef\]](#)
27. Mahanta, B.; Singh, T.; Ranjith, P. Influence of thermal treatment on mode I fracture toughness of certain Indian rocks. *Eng. Geol.* **2016**, *210*, 103–114. [\[CrossRef\]](#)
28. Zhang, F.; Zhao, J.J.; Hu, D.W.; Skoczylas, F.; Shao, J.F. Laboratory investigation on physical and mechanical properties of granite after heating and water-cooling treatment. *Rock Mech. Rock Eng.* **2018**, *5*, 677–694. [\[CrossRef\]](#)
29. Zhang, Z.X.; Kou, S.Q.; Lindqvist, P.; Yu, Y. The relationship between the fracture toughness and tensile strength of rock. In *Strength Theories: Applications, Development and Prospects for 21st Century*; Yu, M., Fan, S.C., Eds.; Science Press: Beijing, China, 1998; pp. 215–219.
30. Kou, S.Q. Effect of thermal cracking damage on the deformation and failure of granite. *Acta Mech. Sin.* **1987**, *19*, 550–556. (In Chinese)
31. Wang, G.D. *Experiment Research on the Effects of Temperature and Viscoelastoplastic Analysis of Beishan Granite*; Xi'an Institute of Science and Technology: Xi'an, China, 2003. (In Chinese)

32. Cheng, J.; Zhao, S.S. *Fracture Mechanics*; Science Press: Beijing, China, 2006. (In Chinese)
33. Xu, Z.L. *Elasticity Mechanics*; Higher Education Press: Beijing, China, 2016. (In Chinese)
34. Erdogan, F.; Sih, G.C. On the crack extension path in plates under plane loading and transverse shear. *ASME J. Basic Eng.* **1963**, *85D*, 519–525. [[CrossRef](#)]
35. Hussain, M.A.; Pu, E.L.; Underwood, J.H. Strain energy release rate for a crack under combined model I and mode II. *ASTM STP* **1974**, *560*, 28. [[CrossRef](#)]
36. Saghafi, H.; Ayatollahi, M.R.; Sistaninia, M. A modified MTS criterion (MMTS) for mixed-mode fracture toughness assessment of brittle materials. *Mater. Sci. Eng. A* **2010**, *527*, 5624–5630. [[CrossRef](#)]
37. Ayatollahi, M.R.; Aliha, M.R.M. Cracked Brazilian disc specimen subjected to mode II deformation. *Eng. Fract. Mech.* **2005**, *72*, 493–503. [[CrossRef](#)]
38. Golshani, A.; Okui, Y.; Oda, M.; Takemura, T. A micromechanical model for brittle failure of rock and its relation to crack growth observed in triaxial compression tests of granite. *Mech. Mater.* **2006**, *38*, 287–303. [[CrossRef](#)]
39. Li, H.B.; Zhao, J.; Li, T.J. Micromechanical modelling of the mechanical properties of a granite under dynamic uniaxial compressive loads. *Int. J. Rock Mech. Min.* **2000**, *37*, 923–935. [[CrossRef](#)]
40. Golshani, A.; Oda, M.; Okui, Y.; Takemura, T.; Munkhtogoo, E. Numerical simulation of the excavation damaged zone around an opening in brittle rock. *Int. J. Rock Mech. Min. Sci.* **2007**, *44*, 835–845. [[CrossRef](#)]
41. Atkinson, C.; Smelser, R.E.; Sanchez, J. Combined mode fracture via the cracked Brazilian disk. *Int. J. Fract.* **1982**, *18*, 279–291.
42. Meredith, P.G.; Atkinson, B.K. Fracture toughness and subcritical crack growth during high-temperature tensile deformation of Westerly granite and Black gabbro. *Phys. Earth Planet. Inter.* **1985**, *39*, 33–51. [[CrossRef](#)]
43. Roy, D.G.; Singh, T.N. Effect of heat-treated and layer orientation on the tensile strength of a crystalline rock under Brazilian test condition. *Rock Mech. Rock Eng.* **2016**, *49*, 1663–1677.
44. Zhang, Z.X.; Yu, J.; Kou, S.Q.; Lindqvist, P.A. Effects of high temperatures on dynamic rock fracture. *Int. J. Rock Mech. Min.* **2001**, *38*, 211–225. [[CrossRef](#)]
45. Lajtai, E.Z. A theoretical and experimental evaluation of the Griffith theory of brittle fracture. *Tectonophysics* **1970**, *11*, 129–156. [[CrossRef](#)]
46. Melin, S. When does a crack grow under mode II conditions? *Int. J. Fract.* **1986**, *30*, 103–114.
47. Kranz, R.L. Crack growth and development during creep of Barre Granite. *Int. J. Rock Mech. Min. Sci. Geomech. Abstr.* **1979**, *16*, 23–35. [[CrossRef](#)]
48. Janach, W. Failure of granite under compression. *Int. J. Rock Mech. Min. Sci. Geomech. Abstr.* **1977**, *14*, 209–215. [[CrossRef](#)]
49. Tapponnier, P.; Brace, W.F. Development of stress-induced microcracks in Westerly granite. *Int. J. Rock Mech. Min. Sci. Geomech. Abstr.* **1976**, *13*, 103–112. [[CrossRef](#)]

